THE EFFECT OF ENGINEERED SURFACES ON THE MECHANICAL PROPERTIES OF TOOL STEELS USED FOR INDUSTRIAL CUTTING TOOLS

A Thesis

Presented to

The Graduate Faculty of The University of Akron

In Partial Fulfillment

of the Requirements for the Degree

Master of Science in Mechanical Engineering

Brandon Strahin

December, 2017

THE EFFECT OF ENGINEERED SURFACES ON THE MECHANICAL PROPERTIES OF TOOL STEELS USED FOR INDUSTRIAL CUTTING TOOLS

Brandon Strahin

Thesis

Approved:

Advisor
Dr. Gary Doll

Co-Advisor
Dr. Paul Shiller

Mechanical Engineering Chair
Dr. Sergio Felicelli

Accepted:

Dean of the College of Engineering
Dr. Donald Visco Jr.

Dean of the Graduate School
Dr. Chand Midha

Date

ABSTRACT

Years of experience have revealed the need for improvements in the performance of cutting tools. One theory to improve cutting tool performance is to reduce shear stresses by applying lubricious engineered surfaces, alter the amount of contact stress transmitted to the substrate material by using a surface with a stiffness that differs from the substrate, and to improve fatigue and wear characteristics of the tool by imparting residual stresses and reducing the average surface roughness by prohibiting crack propagation. This study examined the performance of several engineered surfaces, including superfinishing, thermochemical coatings, and physical vapor deposition coatings. The most significant improvement in performance was due to titanium-doped molybdenum disulfide (Ti-MoS_2), which showed a 370% increase in cycles to failure, had the lowest shear stresses in the surface of the material, and showed the lowest resistance to plastic deformation. The data show a high correlation between the resistance to plastic deformation of the coating and the number of cycles to failure. This suggests that one of the most significant material properties in coatings for cutting tools is the ability to deform with the substrate. The second largest improvement was produced by ferritic nitrocarburizing (FeNC), which provided an increase of 110% in cycles to failure. WC/aC:H decreased cycles to failure by 86%.

DEDICATION

Dedicated to my wife, Bridget, and children, Kaydence, Mason, and Harper, who supported me in the late nights and long hours required to complete this project.

ACKNOWLEDGMENTS

I would like to thank Butech Bliss and Akron Research and Technology for their funding of my research.

I would also like to thank Dr. Gary Doll and Dr. Paul Shiller for their guidance, advice, and patience throughout the learning process.

TABLE OF CONTENTS

LIST OF TABLES

LIST OF FIGURES

CHAPTER I

INTRODUCTION

A need for new advancements in industrial cutting tools has been gleaned from years of industry experience. Industrial cutting tools can be in the form of shear blades, scrap chopper knives, slitter knives, or machining inserts. The need for advances in tooling technology has been exacerbated by the vast advancements made in the steel industry within the past 10 years. The most significant advancement in steel technology has been the development of advanced high-strength steels (AHSS) for the automotive industry. AHSS display combinations of strength and ductility not seen in traditional materials. Rensselar (2011) stated another major concern is the failure of rescue cutting tools when AHSS are encountered by first responders. Industry updates presented by Billur and Altan (2013, 2014a, 2014b) discuss transition-induced plasticity (TRIP) and twinning-induced plasticity (TWIP) AHSS which can exhibit 1.6 GPa tensile strengths while still achieving 40% total elongation. Triplett (2013) and Billur and Altan (2014b) reported AHSS with tensile strengths that can exceed 2.06 GPa. Billur and Altan (2014b) also referenced a new AHSS developed that exhibits 2.1 GPa tensile strength combined with 13% total elongation.

Premature tool failure occurs due to increased wear and increased risk of fracture when processing AHSS (Pinkham, 2014). Increased risk of fracture must also be balanced with the need for adequate strength to handle the high contact stresses experienced during shearing operations. Triplett (2013) states that some tooling manufacturers are using custom chemistries to obtain a good combination of hardness, wear resistance, and toughness to allow for long life without chipping. Success has also been seen when using tools manufactured from cermet, ceramic, and composite materials (Altin, Nalbant, & Taskesen, 2007). However, these materials can be very costly and typically lack the toughness required for cutting operations that see impact loading conditions. It has been estimated that industrial cutting tools account for about $8 billion annually in developed markets (Kopac, 1998). One alternative method to increase the performance of cutting tools is to use engineered surfaces to improve the mechanical properties of the final product. This technique could allow for the use of common grades of tool steels to be used, while obtaining the desired performance from the tooling. It is hypothesized that hard coatings will provide the best improvement in cutting tool performance.

CHAPTER II

LITERATURE REVIEW

Wear and damage on industrial tooling can be caused by several different mechanisms. Theses mechanisms are adhesion, abrasion, diffusion between the tool and workpiece, thermal gradients, load variations, and impact loading (Braghini Junior, Diniz, & Filho, 2009). Tool wear consists of both physical and chemical reactions and consists of approximately 50% abrasion, 20% adhesion, 10% chemical reaction, and 20% other (Kopac, 1998). Impacts to the tool cutting edge can cause cutting edge failure due to cracking, chipping, and plastic deformation (Braghini Junior et al., 2009). In many cases cutting tools that have cracked or chipped cannot be resharpened and must be discarded. Adhesion can best be explained as friction welding between the two materials during contact. Chemical reactions can be reactions between workpiece and cutting tool, with lubricant, or with atmosphere. Traditionally, coatings with high hardness and high thermal stability have been used to provide wear resistance to industrial tooling. Industry trend has been to increase hardness of tool coatings to increase tool life (Rechberger & Dubach, 1993). Titanium nitride, titanium carbide, and aluminum oxide are recommended for dry cutting due to the higher temperatures generated (Kopac, 1998), but chromium nitride, titanium-aluminum nitride, molybdenum disulfide, and amorphous hydrocarbon coatings have also been used (Chinchanikar & Choudhury, 2014; Devillez, Schneider, Dominiak, Dudzinski, & Larrouquere, 2007). Shear blades do not typically see the higher temperatures seen during dry machining and do not require coatings to combat this issue. Plasma nitriding has also seen some success in industrial cutting tools and has been shown to improve the percussive impact resistance of tool steels and decrease the adhesive wear due to sliding and impact (Devi & Mohanty, 1998). Others have also shown that by reducing surface roughness and gas nitriding, the performance of lower cost steels can be improved enough to allow them to be used for tooling in place of higher cost materials (Toboła, Brostow, Czechowski, & Rusek, 2017). These coatings are not suitable for all applications and often require lubrication to reduce friction and prevent failure (Podgornik, Zajec, Bay, & Vižintin, 2011; Rechberger & Dubach, 1993). However, the availability of lubrication in some cutting tool applications is frequently low or non-existent.

One goal of this study was to reduce the possibility of crack initiation and to increase the fatigue strength of the overall material by applying engineered surfaces One form of surface engineering is to modify the surface morphology and induce residual compressive stresses. This can be accomplished by vibratory finishing. Vibratory finishing uses abrasive media moving in random (non-directional) motion in a container to remove surface asperities from the material being processed. Vibratory finishing processes can include centrifugal barrel finishing, tumbling, spinning, barreling, or rotating (Hashimoto, 1999). Vibratory finishing can be used with or without chemical etchants and burnishing agents to assist in the polishing process. Centrifugal barrel finishing is a technique with an increased efficiency provided by the use of centrifugal force generated during operation when compared to traditional rotating barrel finishing. The centrifugal force is generated by the high speed of rotation of the barrel that is filled with abrasives and the materials being finished and can create centripetal accelerations of up to 30G. Since the abrasive media prevents movement, it generates a force between the abrasive media and the material being polished. The optimal polishing efficiency occurs at a rotational speed determined by

$$n = \frac{0.533}{\sqrt{D}} \qquad \text{Eq. 2.1}$$

where n is the rotational speed of the barrel in revolutions per second and D is the diameter of the barrel in meters (Matsunga, 1967). This type of finishing process is highly desirable in many applications because it can produce an isotropic finish, which results in a superior surface. Isotropic finishes are non-directional and contain small surface asperities, which can help improve fatigue strength by reducing crack initiation sites on the surface. Hashimoto (1999) also reports a minimum achievable surface finish that occurs as the average roughness (Ra) approaches 0.06 μm, which can vary slightly based on material and abrasive combinations.

Another form of engineered surfaces is by the use of coatings. Coatings are applied using one of three methods: chemical vapor deposition (CVD), physical vapor deposition (PVD), and thermochemical treatments. This study focuses on PVD and thermochemical processes to produce a variety of coatings. CVD was not used for this study because the high temperatures typical of CVD processes present a high risk of distortion for the tight tolerances used for tooling.

In the PVD process used here, atoms are ejected from a solid target by impacting the surface with energized ions. The advantages of PVD include good adhesion (with proper interlayer), good microstructural control, good compositional control, and deposition temperatures low enough to eliminate tempering and distortion of substrate materials (Bertrand, Savall, & Meunier, 1997). One of the most popular PVD processes is magnetron sputtering due to its efficiency (Ohring, 2002). Magnetron sputtering can deposit pure metals at 1 μm to 3 μm per minute, with a reactive sputtering rate of approximately 60-70% of the pure metal sputtering rate (Nam, Jung, & Han, 2001; Ohring, 2002). Although reactive sputtering is similar to CVD processes, it has the advantage of being able to sputter the metal used for the reaction instead of requiring a volatile metal-containing reactant to be introduced as a precursor (Ohring, 2002). Reactive sputtering is widely used to deposit a variety of tribological coatings commonly used to improve the life of industrial tooling (Sun et al., 2006; Zhang, Yan, Wang, Chen, & Zhang, 2007a). Unbalanced magnetron sputtering is one of the most effective techniques for deposition of high quality tool coatings because of the higher ion current densities and improved ion bombardment achieved from this technique provide high quality, repeatable coatings at good deposition rates (Olaya, Rodil, Muhl, & Sánchez, 2005). Magnetron sputtering is considered unbalanced if the outer ring of magnets is stronger than the central pole

(Kelly & Arnell, 2000). This results in magnetic field lines that are not closed by poles within the magnetron. In systems with multiple magnetrons, poles can either be configured in mirrored (identical) or closed-field (opposing) configurations. In closed-field configurations, the opposing poles of adjacent magnetrons close the magnetic field lines instead of directing them into the chamber walls (Kelly & Arnell, 2000). Since secondary electrons follow these field lines, closed-field configurations generate a high ion density plasma region surrounding the substrate. Figure 2.1 shows a typical four-cathode configuration for a closed-field unbalanced magnetron sputtering system.

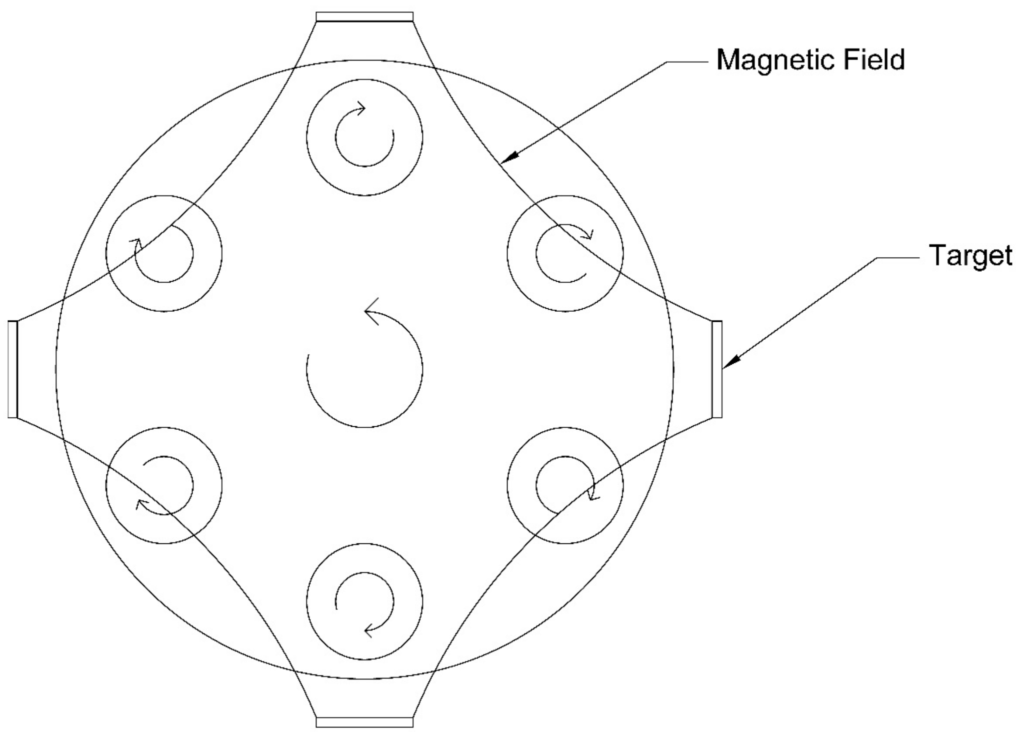

Figure 2.1: Diagram of Closed-Field Unbalanced Magnetron Sputtering Machine.

Chromium nitride has been used as a tool coating for many years. Chromium nitride shows promise in many applications due its good wear resistance, oxidation properties, and corrosion resistance (Bertrand et al., 1997). The wear resistance results from the high hardness (Bertrand et al., 1997). The favorable oxidation properties and corrosion resistance are due to the stability of the thin chromium oxide film that can form on the surface (Bertrand et al., 1997; Sun et al., 2006; Zhang et al., 2007a). Microstructure has a major impact on the mechanical properties displayed by chromium nitride coatings (Zeilinger et al., 2015). One of the most influential processing parameters on microstructure is the nitrogen content during the reactive sputtering process (Zhang et al., 2007a). During sputtering with chromium targets, four structures can be obtained. The structures are pure chromium (0% nitrogen gas), Cr_2N (~20% nitrogen gas), a mixture of CrN and Cr_2N (~40% nitrogen gas), and CrN (~60%+ nitrogen gas) (Olaya et al., 2005; Zhang et al., 2007a). CrN displays a face-centered cubic (rock salt) structure and can have hardness of up to 24 GPa with an indentation modulus of 240 GPa (Sun et al., 2006; Zeilinger et al., 2015; Zhang, Yan, Wang, Chen, & Zhang, 2007b; Zhang et al., 2007a). Cr_2N displays a hexagonal close-packed structure and can exhibit hardness of up to 27 GPa with an indentation modulus of 350 GPa (Han, Tian, Lai, Yu, & Li, 2003). This study is concerned with Cr_2N due to its higher hardness. During scratch testing, Cr_2N delaminates due to its low ductility and poor adhesion and a interlayer must be used to increase adhesion to the substrate (Zhang et al., 2007a).

Another coating used in cutting tools requiring solid lubricants is molybdenum sulfide (MoS_2). MoS_2 has a hexagonal close packed structure that easily shears along basal planes, producing a low coefficient of friction (Banerji, Bhowmick, & Alpas, 2017; Singh et al., 2015; Stoyanov, Strauss, & Chromik, 2012). However, MoS_2 is very sensitive to humidity which restricts the environments in which it can be used (Banerji et al., 2017; Singh et al., 2015). The addition of titanium in MoS_2 produces a titanium-doped molybdenum-disulfide (Ti-MoS_2). The introduction of titanium during the deposition process prevents crystallization of MoS_2, producing an amorphous structure (Banerji et al., 2017; Rigato et al., 1999; Singh et al., 2015). Titanium additions of 5-20 at% improve load-bearing capacity, wear resistance, and friction coefficient in humid air (Rigato et al., 1999; Singh et al., 2015). The tribological improvements are the results of an improvement in mechanical properties and a decrease in interfacial shear stress (Stoyanov, Chromik, Goldbaum, Lince, & Zhang, 2010). Decreasing the interfacial shear stress provides a lower coefficient of friction, lower surface adhesion, and lower shear strengths (Stoyanov et al., 2012). The mechanical property improvements are due to a dispersion strengthening effect caused by titanium in the MoS_2, producing a hardness of about 8 GPa and an indentation modulus of about 170 GPa (Mutyala, Singh, Evans, & Doll, 2015; Singh et al., 2015; Stoyanov et al., 2010). In dry sliding at room temperature, Ti-MoS_2 can form a protective tribofilm by material transfer in sliding contact. This tribofilm was found to consist of nanocrystalline MoS_2 that shears at basal planes that are oriented along the sliding direction in the contact region (Mutyala et al., 2015; Singh et al., 2015; Stoyanov et al., 2012). The tribofilm is able to form after friction generated heat enables titanium to diffuse and crystallization of the MoS_2 occurs. The tribofilm also helps to provide the low coefficient of friction (approximately 0.07) and good wear rates (approximately 5×10^{-5} $mm^3/N \cdot m$ against an alumina counterface) of Ti-MoS_2 (Banerji et al., 2017). The wear rate increases rapidly when temperature starts to exceed 350 °C (Banerji et al., 2017). Since industrial cutting tools do not typically encounter the same work area repeatedly, this wear mechanism may have a detrimental effect on cutting tool life. Provided tool temperatures are kept below 350 °C, Ti-MoS_2 appears to be a potential candidate for improving cutting tool life.

Diamond-like carbon coatings have also been used in many industries, particularly rolling element bearings. These coatings have become desirable in many industries for their excellent properties, including high hardness, high elastic modulus, and low coefficient of friction (Myung, Park, Lee, Hong, & Han, 2005; Podgornik et al., 2011). Diamond-like carbon is composed of sp^2- and sp^3-hybridized carbon bonds and can also contain hydrogen, and/or metal or ceramic precipitates (Mahmoudi, Tury, Hager, & Doll, 2015; Myung et al., 2005). Adding tungsten (W) to form tungsten carbide reinforced diamond-like carbon (WC/aC:H) is one method to increase mechanical properties of the coating such as hardness. This coating can best be described as a metal carbide precipitate-reinforced amorphous hydrocarbon nanocomposite (Mahmoudi et al., 2015). WC/aC:H coatings are able to withstand high contact stresses and have been shown to reduce micropitting and other forms of wear (Mahmoudi et al., 2015). The properties observed are highly sensitive to composition and deposition parameters with ranges of dry friction coefficient of 0.1-0.45, hardness of 10-25 GPa, and an indentation modulus of between 80-210 GPa (Mutyala et al., 2015; Myung et al., 2005; Podgornik et al., 2011). The large range of possible properties make closed-field unbalanced magnetron sputtering a very attractive technique due to its ability to produce coatings with good control, good homogeneity, and high deposition rates (Myung et al., 2005). With proper selection of deposition parameters, WC/aC:H shows potential of improving cutting tool life because of its low coefficient of friction and good load bearing capability.

Thermochemical coating is a surface engineering technique used to alter the chemical composition of the surface of a material by high-temperature reaction of the material and a reactant species. Thermochemical coatings include major processes such as ferritic nitrocarburizing, boronizing, and thermoreactive diffusion. Thermochemical coatings can be formed by salt bath, gas, or plasma, and can provide lower cost alternatives to PVD and CVD processes (Castro, Fernández-Vicente, & Cid, 2007; King, Reynoldson, Brownrigg, & Long, 2005). One of the most common forms for thermochemical treatment is ferritic nitrocarburizing (FeNC). FeNC has several advantages over other processes including lower temperatures, short runtimes, low distortion, and high reproducibility (Castro et al., 2007; Farrahi & Ghadbeigi, 2006; King et al., 2005). During FeNC, nitrogen and carbon (primarily nitrogen) are diffused into the substrate to form a diffusion layer that is metallurgically modified to improve properties, including hardness, fatigue strength, wear resistance, and corrosion resistance (Castro et al., 2007; King et al., 2005). However, the improvement on fatigue strength has been contested by Farrahi & Ghadbeigi (2006), who state that the improvement exists when the cracks initiate internally, but results in a reduction in fatigue strength when cracks initiate at the surface.

When ferritic nitrocarburizing iron based alloys, two layers are formed, a compound layer and a diffusion layer. The diffusion layer consists of primarily interstitially diffused nitrogen in an iron matrix with dispersed metal nitride precipitates (Castro et al., 2007). The diffusion zone is credited with providing the improvement in fatigue strength (Farrahi & Ghadbeigi, 2006; Wells & Shaw, 1985). The compound layer consists of a mixture of cementite, ε-$Fe_{2\text{-}3}$(C,N), and γ'-Fe_4(C,N) (Castro et al., 2007; Wells & Shaw, 1985). In tool steels, the compound layer consist primarily of ε-$Fe_{2\text{-}3}$(C,N) which is beneficial for wear and corrosion properties (Castro et al., 2007; King et al., 2005; Srinivasan, Krishnakumar, & Krishnaraj, 2002; Tarasov, 2001; Wells & Shaw, 1985). FeNC is typically conducted at 570 °C (1058 °F) for 3 to 4 hours to produce a 10 μm to 20 μm compound layer and a 100+ μm diffusion layer (King et al., 2005).

CHAPTER III

RECIPROCATING IMPACT-SLIDING TEST RIG DESIGN

The reciprocating impact-sliding test rig (RISTR) was designed to simulate the tribological contact of an industrial cutting tool for AHSS, such as rotary shear blades and scrap chopper knives under extremely harsh conditions seen in some applications. The RISTR accepts an Ingersoll-Rand 122Max pneumatic hammer regulated to operate at 620.5 kPa using a 19-mm-diameter piston. The pneumatic hammer was used to impact high-strength steel test plates with specially designed chisel specimens.

Initial calculations for the design of the RISTR were performed using equations for general Hertzian contact. The equations for general Hertzian contact are given in Ugural and Fenster's (2013) text on advanced engineering mechanics and applied elasticity (p. 159-170). The calculations for the mean and maximum contact stresses requires the use of Eq. 3.1 (mathematically combined to streamline the calculation process) and Eq. 3.2, respectively.

$$\sigma_{c,mean} = \frac{\sqrt[3]{F}}{\pi c_a c_b \left(\frac{3(1-\nu)^2}{E\left(\frac{1}{r_1}+\frac{1}{r_1'}+\frac{1}{r_2}+\frac{1}{r_2'}\right)} \right)^{\frac{2}{3}}} \qquad \text{Eq. 3.1}$$

$$\sigma_{c,max} = 1.5\sigma_{c,mean} \qquad \text{Eq. 3.2}$$

where r_1 and r_1' are the radii in the planes perpendicular to the plane of contact of the first surface and r_2 and r_2' are the radii in the planes perpendicular to the plane of contact of the second surface. In the above equations, c_a and c_b are constants determined from the calculation of α from Table 3.3 in Ugural and Fenster's (2013) text (p. 169). The calculation of α is performed using Eq. 3.3.

$$\alpha = \cos^{-1}\left(\frac{\left[\left(\frac{1}{r_1}-\frac{1}{r_1'}\right)^2+\left(\frac{1}{r_2}-\frac{1}{r_2'}\right)^2+2\left(\frac{1}{r_1}-\frac{1}{r_1'}\right)\left(\frac{1}{r_2}-\frac{1}{r_2'}\right)\cos 2\theta\right]^{\frac{1}{2}}}{\left(\frac{1}{r_1}+\frac{1}{r_1'}+\frac{1}{r_2}+\frac{1}{r_2'}\right)} \right) \qquad \text{Eq. 3.3}$$

For the design of the RISTR, the variables were chosen to simulate the conditions the cutting tools would be expected to see during the most extreme operating conditions. The radii of the material being cut were taken as ∞ to represent a flat surface giving $1/r_2$ and $1/r'_2$ values of zero. The values used for the maximum and minimum curvatures for the cutting tool were the measured radius of the typical knife hub, r_1=89 mm, and the measured radius of the cutting tool curvature, r'_1=351 mm. The angle between the primary axes, Θ, was taken as 90°. Substituting these values into

Ugural and Fenster's Table 3.3 gives an α=53.5°, and from linear interpolation, c_a=1.654 and c_b=0.630. A standard Poisson's ratio and stiffness for steel were assumed; i.e. ν=0.3 and E=200 GPa. Finally, the force, F, was taken to be the force necessary to cut a piece of AHSS material with thickness, t, of 3 mm and a helix or rake angle, ψ, of 15°. Using trigonometric relationships, the width, w, of the material being cut was found to be (3 mm)/tan(15°), or 11 mm. Schey (2000) gives the cut force necessary to shear a piece of material as:

$$F = C_1 \sigma_{UT} t w \qquad \text{Eq. 3.4}$$

Where C_1 is a ductility coefficient and σ_{UT} is the ultimate tensile strength. Schey reports that C_1 typically falls between 0.65 and 0.85, with higher values corresponding with higher ductility. The value selected for C_1 was 0.85 due to the highly ductile nature of AHSS. Using the AHSS mentioned by Billur and Altan (2014a) with a σ_{UT} of 2.1 GPa gives a cut force, F=60,000 N. Substituting all values determined into Eq. 1 and Eq. 2 gives $\sigma_{c,mean}$=1.8 GPa and $\sigma_{c,max}$=2.7 Pa GPa, respectively.

Next, the radius of the spherical tip on the custom chisel specimen that would be required to produce an equivalent contact stress during the testing had to be determined. This was done by using an equation presented by Ugural (2013) for contact stress of a sphere on a flat plate. Since the desired contact stress was already known from previous calculations, the formula was rearranged to allow for the calculation of the spherical radius, r_s, as shown in Eq. 3.5.

$$r_s = \left(\frac{\sqrt{\frac{1.5F}{\pi \sigma_{c,max}}}}{0.880} \right)^3 \left(\frac{E}{2F} \right) \qquad \text{Eq. 3.5}$$

Eq. 3.5 gives r_S=4.6 mm to produce equivalent mean and maximum contact stresses. It is important to note that Eq. 3.5 assumes a Poisson's ratio of 0.3 and equivalent elastic moduli for both materials.

The RISTR was designed to incorporate sliding through an angle equal to the helix angle. The specimens impacted a flat plate manufactured from AR400 steel which was situated at a -15° angle (relative to horizontal) and allowed to rotate upon impact to an angle of 0° (horizontal). A mechanical stop was used to prevent excessive rotation. This feature was critical to a design that could accurately simulate operating conditions during shearing of the material. The angle of rotation introduces a sliding element to the RISTR. The angle used was chosen based on geometrical layouts to determine the angle that the tooling is engaged in the cut on a rotary cutter such as a drum shear or scrap chopper, although, any type of cutting tool will see significant amounts of sliding during use. During sliding contact, the shear stress produced is a function of the coefficient of friction and the contact stress produced. For this reason, it is suspected that the coefficient of friction plays a large part in tool life. This is especially true in situations where the cutting tools cannot be lubricated or are not lubricated properly. Using trigonometric relationships, the sliding distance, s, was calculated as 8.13 mm. Using an impact frequency, λ, of 3,500 Hz, the horizontal velocity, V_H, was determined by

$V_H = s \cdot \lambda$ Eq. 3.6

and yielded a velocity of 28,445 mm/min. The vertical velocity, V_V, was analyzed using the same approach. The vertical displacement, z, was calculated as 17.02 mm plus 1.56 mm of initial clearance giving a total vertical displacement of 18.61 mm. Substituting into Eq. 3.6 and using the same impact frequency gives a vertical velocity, V_V, of 65,126 mm/min. Figure 3.1 shows a graphical representation of the sliding calculations.

The RISTR was equipped with a flow controller, pressure regulator, and in-line air tool lubricator to ensure consistent performance throughout the entire testing duration. The pressure regulator was set to 620.5 kPa90 psi. The finished RISTR is shown in Figure 3.2.

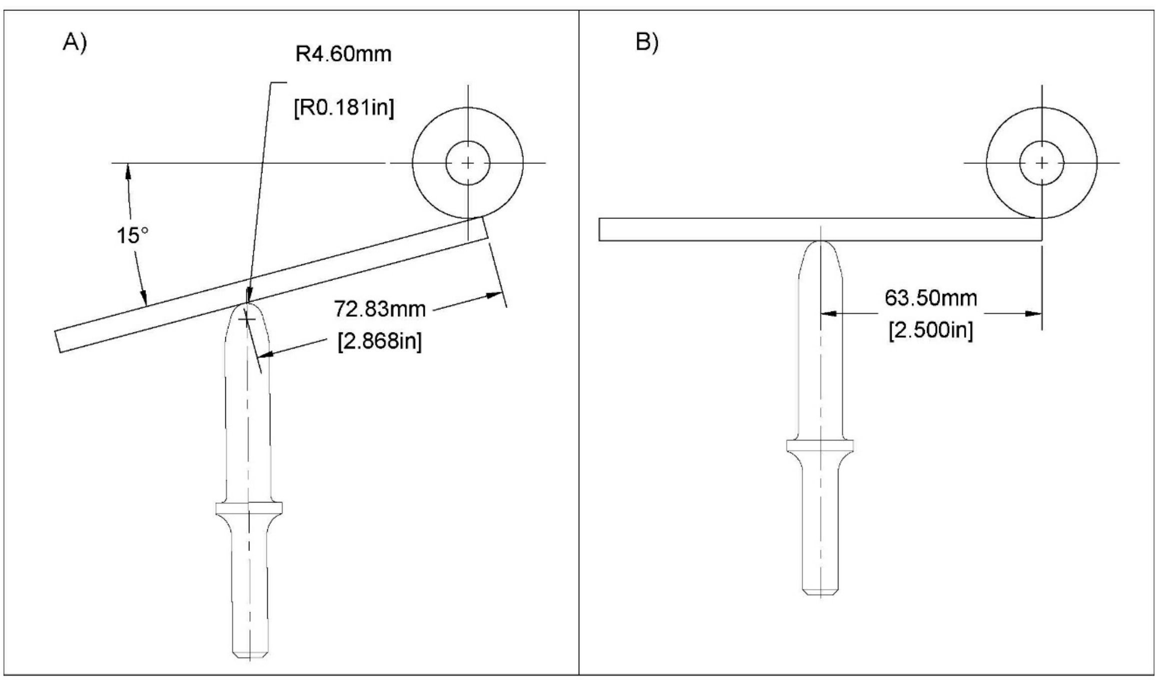

Figure 3.1: Diagram of the RISTR showing a graphical representation of the sliding calculations.

Figure 3.2: Reciprocating impact-sliding test rig.

CHAPTER IV

EXPERIMENTAL PROCEDURES

Although CPM 9V tool steel is commonly used in industrial cutting tool applications, one of the primary modes of failure observed with this material has been plastic deformation. This has motivated the need for tooling fabricated from a material that could obtain a higher hardness, but would not fracture easily during operation. AISI M2 tool steel was selected as the alternative material because of its much higher obtainable hardness and moderate toughness. The composition of the material used is shown in Table 4.1. Impurities of less than 0.01 wt.% are not included in this table. The specimens were austenitized in vacuum at 1,200°C, positive pressure nitrogen quenched at 5 Bar, and double tempered at 540°C to obtain a desired hardness of 65 HRC.

One process of surface engineering is to modify the surface roughness. The tools inspected had a surface roughness of approximately 0.8 μm Ra. Control specimens were studied using a 0.8 μm Ra surface finish. The surface finish on all

Table 4.1: Chemical composition of AISI M2 used for experimentation.

Chemical	**C**	**Cr**	**Mo**	**Mn**	**P**	**Si**	**V**	**W**	**Ni+Cu**	**Fe**
wt.%	0.82	3.99	.27	4.55	0.02	0.36	1.80	5.66	0.47	Bal.

other specimens was reduced to a 0.2 µm Ra to study the treatments. Reduction of surface roughness was done by placing the specimens in a chemical vibratory finishing bowl with Chemtrol 440 etching solution pre-diluted with water at a 57:1 ratio for two hours. The specimens were then exposed to a continuous supply of burnishing solution composed of Chemtrol 220 diluted with water at a 57:1 ratio for two hours from a low volume pump. After vibratory bowl finishing was complete, the specimens were mass finished in a Mikronite centrifugal barrel finisher for 60 minutes to polish and induce residual compressive stresses into the surface of the material.

Ferritic Nitrocarburizing

The ferritic nitrocarburizing (FeNC) specimens for testing were produced using a proprietary chemistry originally developed for the Black Nitride process developed by H&M Metal processing in Akron, OH (used with permission). The specimens were ferritic nitrocarburized at 580°C for 3 hours. This process produced a white layer 4.5 µm thick and an average total diffusion depth of 41 µm. The hardness of the layer produced was checked using a Microton hardness tester at 1571 HV using a 100-g load. Figure 2.1 shows the FeNC diffusion coating with white layer and black layer thickness measurements.

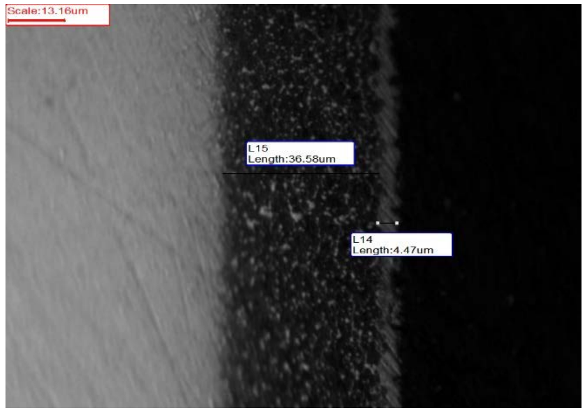

Figure 4.1: Optical microscope image showing diffusion depth of white and black layers of ferritic nitrocarburizing on AISI M2 tool steel.

PVD Coatings

All PVD coatings used for experimentation were produced in the Timken Engineered Surfaces Laboratories at The University of Akron using closed-field unbalanced magnetron sputtering (CFUMS). Coatings were deposited onto AISI M2 tool steel substrates. The substrates consisted of 6-mm diameter balls and custom designed impact tribometer chisels. Prior to coating, specimens were placed through the superfinishing processes to reduce surface roughness. After the superfinishing process, specimens were degreased in Proguard 142 HT solvent with agitation before being ultrasonically cleaned in an alkaline solution to remove any additional contaminants. The cleaning process was completed on a Crest cleaning line with two 5-minute ultrasonic washes in Chemcrest 275 at 65.6 °C, followed by two 5-minute ultrasonic rinses in Chemcrest 77 at 65.6 °C. The process was finished by rinsing in deionized water and drying in air at 107.2 °C.

After being cleaned, the substrates were immediately placing into the deposition chamber. The chamber was evacuated to a base pressure below $1X10^{-6}$

Torr prior to beginning the deposition process. High-purity (99.999%) argon gas was flowed into the chamber at 50 sccm for the duration of the deposition. Interlayers of approximately 100 nm were used for adhesion. Cr was selected as the interlayer material for Cr_2N and WC/aC:H and Ti was selected as the interlayer material for Ti-MoS_2.

Figures 4.2, 4.3 and 4.4 show the thickness of each coating measured using an optical microscope. The thickness measured for each coating was 1.4 μm, 2.2 μm, and 1.1 μm for the titanium-doped molybdenum disulfide (Ti-MoS_2), tungsten-doped diamond-like carbon (WC/aC:H), and chromium nitride (Cr_2N), respectively. Table 4.2 shows the properties of the selected coatings used for this study.

Table 4.2: Properties of selected coatings.

Engineered Surface	**Hardness (GPa)**	**Indentation Modulus (GPa)**	**Thickness (μm)**
FeNC	15.3	272	41 Diffusion 4.5 Compound
Ti-MoS_2	7.9	172	1.4
WC/aC:H	14	130	2.2
Cr_2N	20	280	1.1

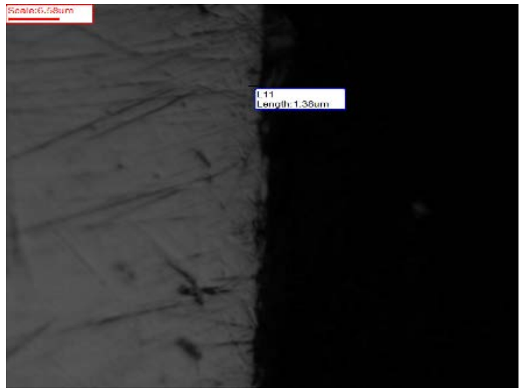

Figure 4.2: Optical microscope image of Ti-MoS_2 coating thickness.

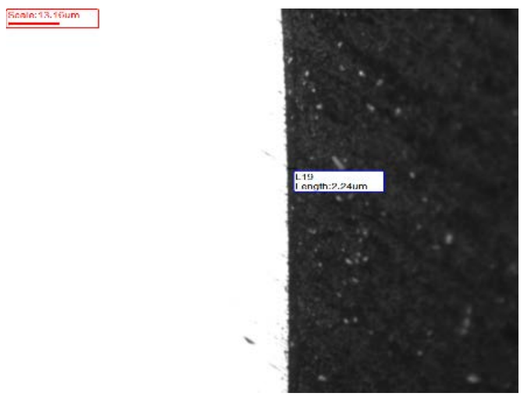

Figure 4.3: Optical microscope image of WC/aC:H coating thickness.

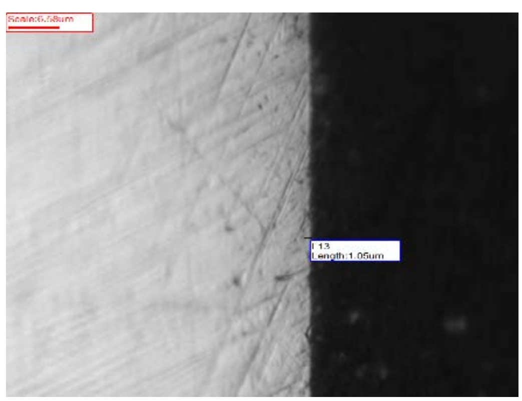

Figure 4.4: Optical microscope image of Cr_2N coating thickness.

Mechanical Testing

Charpy Impact Testing

Charpy impact testing uses a striker to impact a specimen supported between two anvils to produce a multi-axial stress with a high loading rate (ASTM International, 2012). Although the components of crack initiation and crack propagation cannot be separated with a V-notch type specimen, Charpy impact testing can accurately predict brittle fracture when correlated with adequate service experience (ASM International, 2000). Charpy impact testing was completed using an Instron 600MPX testing machine. Specimens were machine as standard Charpy V-Notch impact specimens and conformed to ASTM E23. All specimens were tested at room temperature to simulate actual operating conditions of the cutting tools.

Reciprocating Impact-Sliding Test Rig

Specimens for the RISTR were manufactured from AISI M2 tool steel and engineered surfaces were applied using the procedures described in previous sections. The pneumatic hammer operated at 3,500 impacts per minute and each test was run for 86-second (5,000-cycle) intervals. The spherical tips of each specimen were scanned using a Zygo NewView 7300 optical interferometer before each test and after each 5,000-cycle interval. The specimens were scanned for failure criteria after the initial test, then tested at 5,000-cycle intervals until failure, being examined for failure criteria using an optical interferometer after each interval. A specimen was deemed to have failed if the radius of the tip exceeded 9 mm, or if there was evidence of chipping, cracking, or spalling on the spherical tip during the interval scans. Special attention was paid to pre-existing defects to prevent a specimen being deemed as failed from an initial flaw. A new plate specimen was used for each chisel specimen, and was replaced every 100,000 cycles to maintain contact stresses during testing.

Pin-on-Disk Testing

The pin-on-disk testing was performed on a CSEM high temperature tribometer. The test parameters used were selected to simulate the wear conditions typically seen in many industrial cutting tool applications. The tests were performed using coated 6-mm balls made from AISI M2 tool steel using a 2-N load. This combination produced a maximum and mean contact stress of 0.83 GPa and 0.55 GPa, respectively. The disks were manufactured from AR400 steel. The tests were run dry under atmospheric conditions at 10 cm/s for distances of 100 m, 200 m, and 400 m using radii of 10 mm, 15 mm, and 20 mm, respectively.

CHAPTER V

RESULTS AND DISCUSSION

The selected coatings were put through mechanical testing as described in the previous section. Figure 5.1 shows the Charpy impact data. The data show that while the PVD coatings did not cause a statistical change in the fracture toughness of the specimen, the specimens with the FeNC lowered the impact toughness by approximately 50%. These data provide information needed to predict how the material will fracture once initiation of a crack on the cutting edge occurs. Coatings that do not cause a decrease in impact toughness appear to be better candidates for cutting tools.

The RISTR was developed to mimic the environment that many cutting tools are exposed to during normal operation. Figure 5.2 shows the data collected from the modified impact tribometer. One of the WC/aC:H specimens was damaged during the manufacturing process and did not provide valid data. These data were omitted from the analysis. The data in Figure 5.2 show that Ti-MoS_2 produced the largest increase in the number of cycles to failure with approximately 370% improvement.

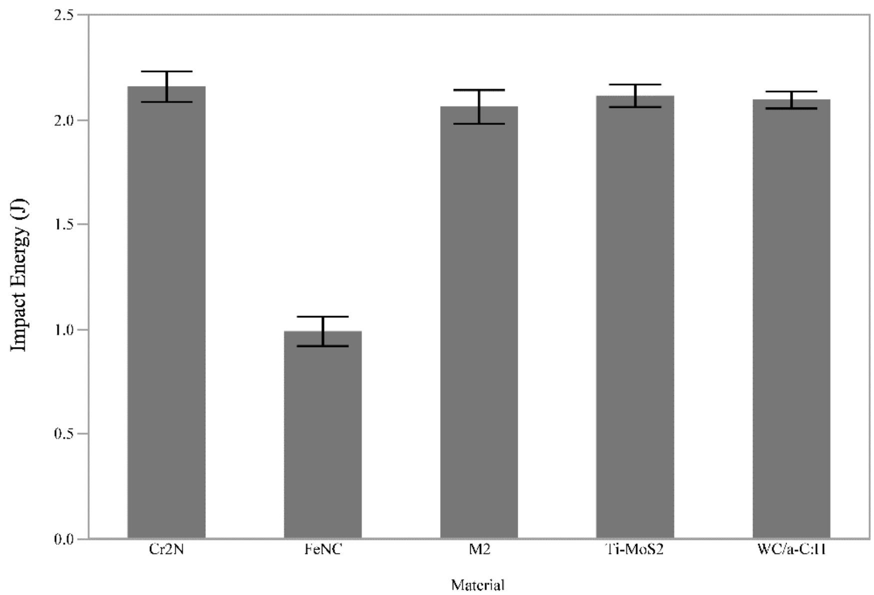

Figure 5.1: Charpy impact data for coated and uncoated specimens.

This was followed by FeNC with approximately 86% improvement, and Cr_2N with approximately 58% improvement. RISTR testing agrees with data presented by Rechberger et al (1993) that observed that soft coatings demonstrate a more significant improvement than hard coatings at very high loads. M2, Cr_2N, and Ti-MoS_2 failed due to spalling of the substrate, causing failure of the coating on coated specimens. Ti-MoS_2 also had cracking originating at the site of the spall. This is most likely caused by surface fatigue from the high contact stresses.

Superfinishing the specimens did not make a difference in the number of cycles to failure. This is most likely caused by high contact stresses creating a "peening-like" effect. This effect smooths out surface asperities during testing, creating a superfinished surface on the specimens without an additional process. With both the baseline and superfinished specimens having an ultra-smooth testing surface after a short break-in period, the data from the specimens are almost identical and exhibit no difference in the cycles to failure.

Only WC/aC:H caused a decrease in the number of cycles to failure, with an observed loss of approximately 86%. This observation of fracture that propagates into the substrate is consistent with results of a study by Mahmoudi, Tury, Hager, and Doll (2015) that reported that the WC/aC:H coating would fracture under high contact stresses (over 2 GPa) during cyclic Hertzian contact. The WC/aC:H coating in this test fractured prior to the completion of 10,000 cycles for all specimens. Overall, the WC/aC:H caused a decrease in tool performance.

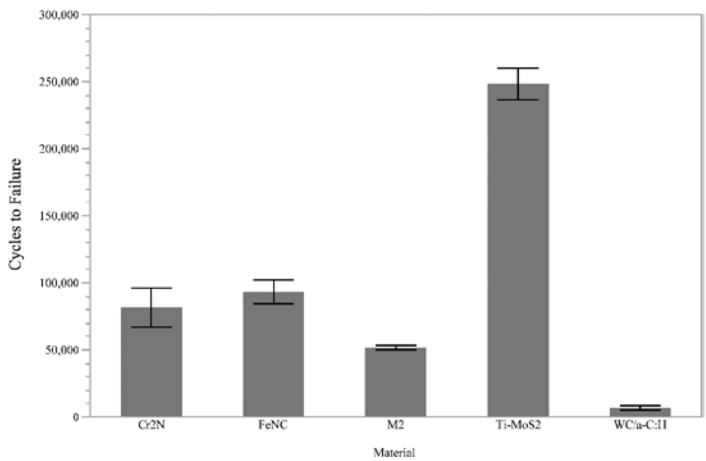

Figure 5.2: Average cycles to failure from reciprocating impact-sliding testing.

The data from RISTR testing were examined for correlations to various mechanical relationships using JMP Pro 12 analysis software and was found to have a high correlation to the resistance of the coating to plastic deformation. The resistance to plastic deformation is defined as

$R = \frac{H^3}{E^2}$ Eq. 5.1

where R is the resistance to plastic deformation, H is the hardness of the coating, and E is the indentation modulus of the coating (Leyland & Matthews, 2000). More specifically, the data scale as the inverse of the resistance to plastic deformation. This implies that the more easily a coating can deform with the substrate under very high contact stresses, the more durable it will be under high cyclic impact forces. This relationship is demonstrated graphically in Fig. 5.3. The generalized equation derived from the data fit is

$N_{Failure} = \frac{3970\ GPa}{R} + 13{,}162$ Eq. 5.2

and had a coefficient of determination (R^2 value) of 0.914.

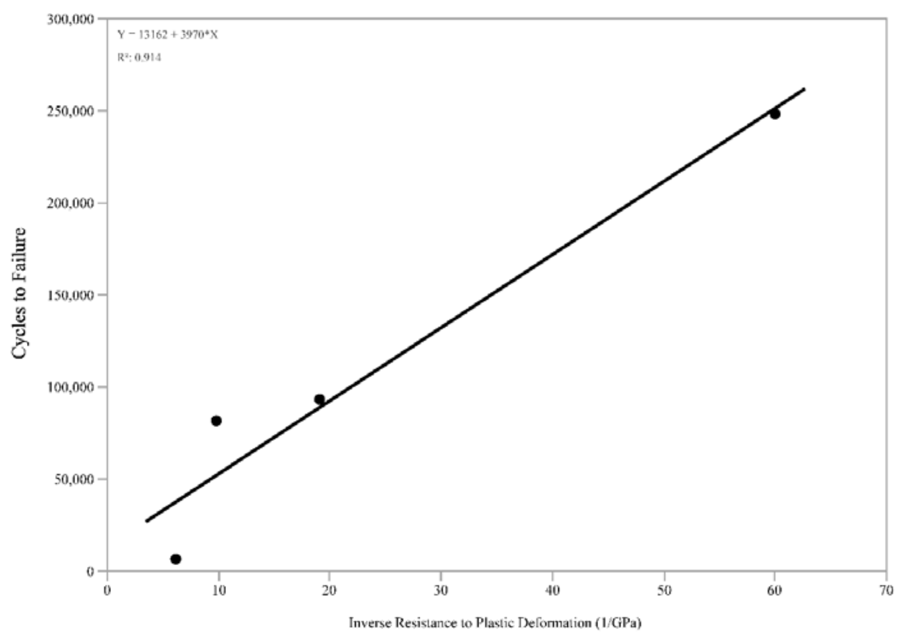

Figure 5.3: RISTR data plotted against the coatings resistance to plastic deformation.

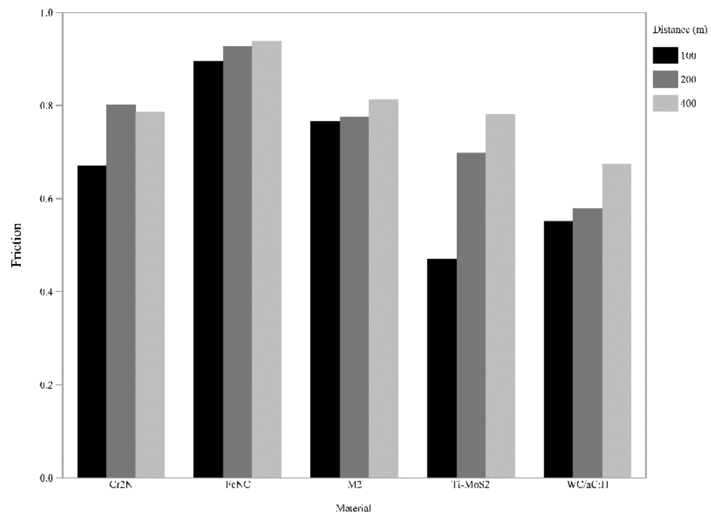

Figure 5.4: Friction coefficients for each material pair measured in situ.

Friction coefficients were measured in unidirectional sliding in dry contact for five material pairings. Figure 5.4 shows the average values of the friction for each of the distances tested. Although the tests wore though the coatings completely, both WC/aC:H and Ti-MoS_2 continued to provide some lubricity and allowed the system to operate at a lower friction than the M2/AR400 pairing.

Figure 5.5 shows wear volume of the balls in mm^3 for each pairing plotted against dissipated energy (J). Values of the slopes (α) of the best linear fits to the data were $5.44x10^{-8}$ mm^3/J (Cr_2N), $5.96x10^{-7}$ mm^3/J (WC/a-C:H), $6.70x10^{-7}$ mm^3/J (FeNC), $7.57x10^{-7}$ mm^3/J (M2), and $8.23x10^{-7}$ mm^3/J (Ti-MoS_2). The α values or wear coefficients scaled with the hardness of the chisel surface (H = 8.2 GPa for M2 steel). Within the Archard formalism, wear volume (V) is related to dissipated energy (E_d) and surface hardness as

$$V = k\left(\frac{E_d}{H}\right). \quad \text{Eq. 5.3}$$

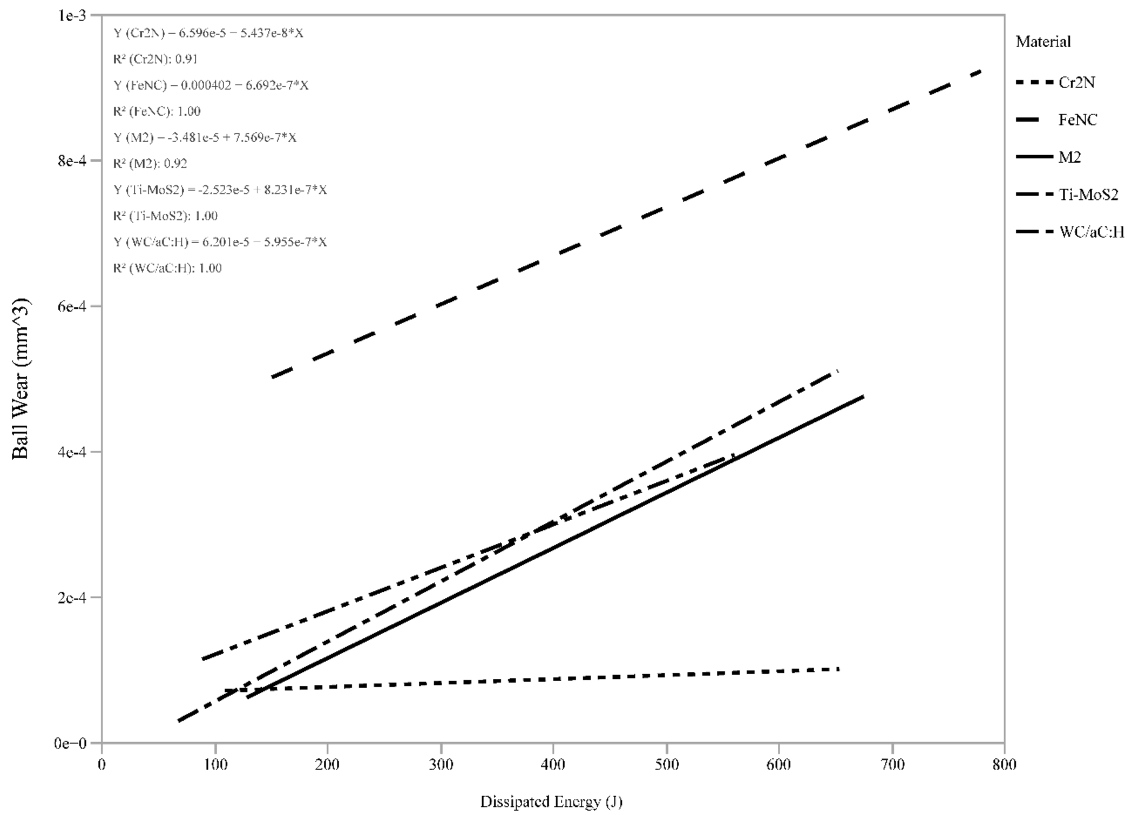

Figure 5.5: Plot of dissipated energy and ball wear used to determine wear coefficients.

Evaluation of the collective results from the wear and impact testing indicated that the ability of the coating to accommodate plastic deformation was the most critical attribute for a coating on M2 tool steel to cut AHSS. Although the Cr_2N coating showed significant wear resistance over untreated M2 steel, only minor improvements in cycles to failure were achieved with this coating. On the other hand, while the Ti-MoS_2 coating was less wear resistant than the untreated steel, it provided the largest increase in cycles to failure. Although both Ti-MoS_2 and WC/aC:H coatings had lower friction against AR400 than the untreated M2 balls, Ti-MoS_2 increased while WC/aC:H decreased the cycles to failure. This suggests that the friction coefficient has little impact on the number of cycles to failure.

CHAPTER VI

CONCLUSION

Premature failure of cutting tools can cause costly downtime in industrial processing lines or even delay critical lifesaving procedures during rescue operations. Many factors can impact the performance of cutting tools. Several properties were examined during this study. It was found that cutting tool performance can be improved by the use of an engineered surface and can allow for the use of less expensive substrate materials provided the overall bulk material can exhibit certain characteristics. The optimal cutting tool will have the best combination of required characteristics including:

- Low coefficient of friction.
- Low resistance to plastic deformation.
- Good impact toughness.
- Good response to Hertzian cyclic stresses.
- Good wear resistance.

Many engineered surfaces were examined during this study to see which could meet the necessary criteria. It was found that the best materials for improving the cycles to failure of industrial cutting tools have a low resistance to plastic deformation and that the resistance to plastic deformation had the largest impact on cutting tool performance of the properties examined. The best performance achieved in this study was produced by Ti-MoS_2, which had the highest wear rate (α value), but exhibited the lowest coefficient of friction, and thus the lowest shear stresses generated during sliding contact. Ti-Mos_2 also had the lowest resistance to plastic deformation, and did not lower the impact toughness.

Although Ti-MoS_2 provided an improvement of 370% over the baseline M2 material, appropriate material selection needs to be completed on a case by case basis to ensure that the proper substrate material is selected. A coating should also be selected that has a low resistance to plastic deformation (low H^3/E^2), but also has adequate wear resistance and impact toughness to allow for extended use in the application selected.

REFERENCES

Altin, A., Nalbant, M., & Taskesen, A. (2007). The effects of cutting speed on tool wear and tool life when machining Inconel 718 with ceramic tools. *Materials & Design*, *28*(9), 2518–2522. https://doi.org/10.1016/j.matdes.2006.09.004

Banerji, A., Bhowmick, S., & Alpas, A. T. (2017). Role of temperature on tribological behaviour of Ti containing MoS 2 coating against aluminum alloys. *Surface and Coatings Technology*, *314*, 2–12. https://doi.org/10.1016/j.surfcoat.2016.09.044

Bertrand, G., Savall, C., & Meunier, C. (1997). Properties of reactively RF magnetron-sputtered chromium nitride coatings. *Surface and Coatings Technology*, *96*(2–3), 323–329.

Billur, E., & Altan, T. (2013, December). Three Generations of Advanced High-Strength Steels for Automotive Applications, Part I. *Stamping Journal*, 16–17.

Billur, E., & Altan, T. (2014a, February). Three Generations of Advanced High-Strength Steels for Automotive Applications, Part II. *Stamping Journal*, 12–13.

Billur, E., & Altan, T. (2014b, April). Three Generations of Advanced High-Strength Steels for Automotive Applications, Part III. *Stamping Journal*, 12–13.

Braghini Junior, A., Diniz, A. E., & Filho, F. T. (2009). Tool wear and tool life in end milling of 15–5 PH stainless steel under different cooling and lubrication conditions. *The International Journal of Advanced Manufacturing Technology*, *43*(7–8), 756–764. https://doi.org/10.1007/s00170-008-1744-6

Castro, G., Fernández-Vicente, A., & Cid, J. (2007). Influence of the nitriding time in the wear behaviour of an AISI H13 steel during a crankshaft forging process. *Wear*, *263*(7–12), 1375–1385. https://doi.org/10.1016/j.wear.2007.02.007

Chinchanikar, S., & Choudhury, S. K. (2014). Evaluation of Chip-tool Interface Temperature: Effect of Tool Coating and Cutting Parameters during Turning Hardened AISI 4340 Steel. *Procedia Materials Science*, *6*, 996–1005. https://doi.org/10.1016/j.mspro.2014.07.170

Devi, M. U., & Mohanty, O. N. (1998). Plasma-nitriding of tool steels for combined percussive impact and rolling fatigue wear applications. *Surface and Coatings Technology*, *107*(1), 55–64.

Devillez, A., Schneider, F., Dominiak, S., Dudzinski, D., & Larrouquere, D. (2007). Cutting forces and wear in dry machining of Inconel 718 with coated carbide tools. *Wear*, *262*(7–8), 931–942. https://doi.org/10.1016/j.wear.2006.10.009

Farrahi, G. H., & Ghadbeigi, H. (2006). An investigation into the effect of various surface treatments on fatigue life of a tool steel. *Journal of Materials Processing Technology*, *174*(1–3), 318–324. https://doi.org/10.1016/j.jmatprotec.2006.01.014

Han, Z., Tian, J., Lai, Q., Yu, X., & Li, G. (2003). Effect of N 2 partial pressure on the microstructure and mechanical properties of magnetron sputtered CrN x films. *Surface and Coatings Technology*, *162*(2), 189–193.

Hashimoto, F. (1999, February 23). *5,873,770*. Washington D.C.: U.S. Patent and Trademark Office.

Kelly, P. J., & Arnell, R. D. (2000). Magnetron sputtering: a review of recent developments and applications. *Vacuum*, *56*(3), 159–172.

King, P. C., Reynoldson, R. W., Brownrigg, A., & Long, J. M. (2005). Ferritic nitrocarburising of tool steels. *Surface Engineering*, *21*(2), 86–98. https://doi.org/10.1179/174329405X40920

Kopac, J. (1998). Influence of cutting material and coating on tool quality and tool life. *Journal of Materials Processing Technology*, *78*, 95–103.

Leyland, A., & Matthews, A. (Eds.). (2000). On the Significance of the H/E Ratio in Wear Control: A Matrix Composite Coating Approach to Optimized Tribological Behaviour. *Wear*, 1–11.

Mahmoudi, B., Tury, B., Hager, C. H., & Doll, G. L. (2015). Effects of Black Oxide and a WC/a-C:H Coating on the Micropitting of SAE 52100 Bearing Steel. *Tribology Letters*, *58*(2). https://doi.org/10.1007/s11249-015-0494-5

Matsunga, M. (1967). Theory and Experiments on Centrifugal Barrel Finishing. *The International Journal of Production Research*, *5*(4), 275–287.

Mutyala, K. C., Singh, H., Evans, R. D., & Doll, G. L. (2015). Deposition, characterization, and performance of tribological coatings on spherical rolling elements. *Surface and Coatings Technology*, *284*, 302–309. https://doi.org/10.1016/j.surfcoat.2015.06.075

Myung, H. S., Park, Y. S., Lee, J. W., Hong, B., & Han, J. G. (2005). Structures and mechanical properties of diamond like carbon films prepared by closed-field unbalanced magnetron sputtering. *Thin Solid Films*, *475*(1–2), 303–307. https://doi.org/10.1016/j.tsf.2004.07.017

Nam, K. H., Jung, Y. M., & Han, J. G. (2001). A comparative study of microstructure and mechanical properties for CrN x films with various deposition rates by magnetron sputtering. *Surface and Coatings Technology*, *142*, 1012–1016.

Ohring, M. (2002). Plasma and Ion Beam Processing of Thin Films. In *Materials Science of Thin Films: Deposition and Structure* (2nd ed., pp. 203–275). San Diego, CA: Academic Press.

Olaya, J. J., Rodil, S. E., Muhl, S., & Sánchez, E. (2005). Comparative study of chromium nitride coatings deposited by unbalanced and balanced magnetron sputtering. *Thin Solid Films*, *474*(1–2), 119–126. https://doi.org/10.1016/j.tsf.2004.08.067

Pinkham, M. (2014, February). Tollers Tooling Up for High-Strength Steel. *Metal Center News*, 18–24.

Podgornik, B., Zajec, B., Bay, N., & Vižintin, J. (2011). Application of hard coatings for blanking and piercing tools. *Wear*, *270*(11–12), 850–856. https://doi.org/10.1016/j.wear.2011.02.013

Rechberger, J., Brunner, P., & Dubach, R. (1993). High performance cutting tools with a solid lubricant physically vapour-deposited coating. *Surface and Coatings Technology*, *62*, 393–398.

Rechberger, J., & Dubach, R. (1993). Soft physical vapour deposition coatings - a new coating family for high performance cutting tools. *Surface and Coatings Technology*, *60*, 584–586.

Rigato, V., Maggioni, G., Boscarino, D., Sangaletti, L., Depero, L., Fox, V. C., … Santini, C. (1999). A study of the structural and mechanical properties of Ti= MoS 2 coatings deposited by closed field unbalanced magnetron sputter ion plating. *Surface and Coatings Technology*, *116*, 176–183.

Schey, J. (2000). Shearing. In *Introduction to Manufacturing Processes* (3rd ed., pp. 388–397). McGraw-Hill.

Singh, H., Mutyala, K. C., Mohseni, H., Scharf, T. W., Evans, R. D., & Doll, G. L. (2015). Tribological Performance and Coating Characteristics of Sputter-Deposited Ti-

Doped MoS_2 in Rolling and Sliding Contact. *Tribology Transactions*, *58*(5), 767–777. https://doi.org/10.1080/10402004.2015.1015758

Srinivasan, P. B., Krishnakumar, C. V., & Krishnaraj, N. (2002). Sliding wear behavior of salt bath nitrocarburized medium carbon steel. *Journal of Materials Engineering and Performance*, *11*(5), 509–515.

Stoyanov, P., Chromik, R. R., Goldbaum, D., Lince, J. R., & Zhang, X. (2010). Microtribological Performance of Au–MoS2 and Ti–MoS2 Coatings with Varying Contact Pressure. *Tribology Letters*, *40*(1), 199–211. https://doi.org/10.1007/s11249-010-9657-6

Stoyanov, P., Strauss, H. W., & Chromik, R. R. (2012). Scaling effects between micro- and macro-tribology for a Ti–MoS2 coating. *Wear*, *274–275*, 149–161. https://doi.org/10.1016/j.wear.2011.08.021

Sun, C.-C., Lee, S.-C., Dai, S.-B., Fu, Y.-S., Wang, Y.-C., & Lee, Y.-H. (2006). Surface free energy of CrNx films deposited using closed field unbalanced magnetron sputtering. *Applied Surface Science*, *252*(23), 8295–8300. https://doi.org/10.1016/j.apsusc.2005.10.055

Tarasov, A. N. (2001). Cutting and shaping tools from nitrocarburized high-speed steels: A possible alternative to hard-alloy tools. *Metal Science and Heat Treatment*, *43*(3), 169–172.

Toboła, D., Brostow, W., Czechowski, K., & Rusek, P. (2017). Improvement of wear resistance of some cold working tool steels. *Wear*, *382–383*, 29–39. https://doi.org/10.1016/j.wear.2017.03.023

Triplett, T. (2013, July). Ahead of the AHSS Curve. *Metal Center News*, 26–29.

Ugural, A., & Fenster, S. (2013). Contact Stresses. In *Advanced Mechanics of Materials and Applied Elasticity* (5th ed., pp. 159–170). Westford, MA: Prentice Hall.

Van Rensselar, J. (2011, July). The Riddle of Steel: A-UHSS. *Tribology & Lubrication Technology*, 38–46.

Wells, A., & Shaw, M. P. (1985). An investigation into dry sliding wear behaviour of the ferritic nitrocarburized surface of a plain low carbon steel. *Wear*, *103*(1), 29–42.

Zeilinger, A., Daniel, R., Schöberl, T., Stefenelli, M., Sartory, B., Keckes, J., & Mitterer, C. (2015). Resolving depth evolution of microstructure and hardness in sputtered CrN film. *Thin Solid Films*, *581*, 75–79. https://doi.org/10.1016/j.tsf.2014.10.106

Zhang, G. A., Yan, P. X., Wang, P., Chen, Y. M., & Zhang, J. Y. (2007a). Influence of nitrogen content on the structural, electrical and mechanical properties of CrNx thin films. *Materials Science and Engineering: A*, *460–461*, 301–305. https://doi.org/10.1016/j.msea.2007.01.149

Zhang, G. A., Yan, P. X., Wang, P., Chen, Y. M., & Zhang, J. Y. (2007b). The structure and tribological behaviors of CrN and Cr–Ti–N coatings. *Applied Surface Science*, *253*(18), 7353–7359. https://doi.org/10.1016/j.apsusc.2007.02.061